WARSAW UNIVERSITY OF TECHNOLOGY Index 351733
FACULTY OF CIVIL ENGINEERING
COMMITTEE FOR CIVIL AND WATER ENGINEERING
POLISH ACADEMY OF SCIENCES ISSN 1230-2945

DOI: 10.24425/ace.2026.157481

ARCHIVES OF CIVIL ENGINEERING

Vol. LXXII ISSUE 1 2026

pp. 393–403

Research paper

Research on deep excavation deformation prediction model based on machine learning algorithms

Yujun Guo[1], Xu Yang[2], Yansheng Deng[3]

Abstract: Due to the continuous rise of urban underground space development, there has been an increasing number of deep excavation project in recent years, in China. The complexity of hydrogeological conditions and surrounding environment makes it difficult to calculate the deformation of excavation wall caused by deep excavation. Based on the monitoring data during the entire deep excavation process, four data-driven machine-learning algorithms were developed and evaluated in this study to predict deep horizontal displacement (DHD) of excavation wall considering the excavation process and spatial effect. The results showed that the XGBoost algorithm has the best performance, with an *RMSE* of 2.3397, an *MAE* of 1.5732 and R^2 of 0.9088. Furthermore, it has higher accuracy in predicting the DHD at the corners, followed by the deformation caused by excavation stage 2. It can be seen that the machine-learning algorithms can be a potential tool for predicting DHD caused by deep excavation in practical engineering.

Keywords: deep excavation, deformation prediction, machine learning algorithm

[1]MSc., Eng., The First Geological Brigade of Jiangsu Geological Bureau, Nanjing, 210041, China, e-mail: 568895351@qq.com, ORCID: 0009-0007-2475-5917

[2]MSc., Sen. Eng., The First Geological Brigade of Jiangsu Geological Bureau, Nanjing, 210041, China, e-mail: 981907827@qq.com, ORCID: 0009-0004-0703-418X

[3]PhD., Lecturer, School of Civil Engineering and Architecture, Zhejiang University of Science and Technology, Hangzhou, 310023, China, e-mail: ysdeng@zust.edu.cn, ORCID: 0000-0002-4329-1827

1. Introduction

With the continuous improvement of urbanization level, the contradiction between the increasing urban population and limited land resources is becoming increasingly prominent in China. To alleviate this problem, urban underground space has been developed and utilized, such as urban pipe galleries, underground transportation, underground parking lots, and so on. Especially in recent years, a large number of subway constructions have been carried out in China. Deep foundation excavation seems to easily cause ground subsidence or damage of surrounding buildings and infrastructure, and even collapse and casualties [1]. Therefore, the research on deformation prediction induced by deep excavation is of great significance and has attracted widespread attention from engineers and scholars [2]. The traditional method on deformation caused by deep excavation is mainly based on monitoring data analysis. With the development of computers and numerical technology, the numerical simulation method has been widely applied to predict the deformation induced by excavation and other factors [3–5]. [6] estimated the maximum horizontal displacement around the power station caverns with artificial neural network. [7] verified the feasibility of random-forest algorithm for prediction settlement caused by shield-driven tunnel excavation. [8] used finite element analysis to simulate the deep excavation for evaluating wall deflections and performance. To evaluate the effects of soft clay anisotropy on the diaphragm wall deflections in the braced deep excavation, [9] developed surrogate models via ensemble learning methods, like the extreme gradient boosting, random forest regression, to predict the wall deformation. In recent years, [10] proposed and verified an improved optimization algorithm of supply and demand-exponential power product foundation pit deformation prediction model based on the settlement induced by excavation of three foundation pits. [11] adopted the LSTM network model to predict the horizontal and vertical displacement of retaining pile and column in deep excavation. [12] combined digital twins and machine learning to investigate the structural health monitoring of bridges. [13] employed six machine-learning methods to predict the enclosure deformation of deep foundation pits and their performance was systematically investigated using K-Fold cross validation.

Although some significant results have been obtained on deformation prediction caused by deep excavation, it is still important to study the prediction method of deformation of excavation wall during deep excavation due to the complexity of factors, especially the time-space effect. In this work, four mainstream machine-learning algorithms were employed to build prediction model based on selected three features. Then, a dataset of 1362 was used to evaluate the accuracy of models, and their performance was analyzed systematically with various assessment parameters.

2. Methodology

Machine-learning models have been developed rapidly and widely applied in various fields in recent years. In this work, four mainstream machine-learning algorithms were employed to build prediction model for DHD shown in Table 1.

Table 1. Description of machine-learning methods adopted in this work

No.	Machine-learning method	Clarification
1	Decision Tree (DT) [14, 15]	DT is a tree structured model, which works by recursively partitioning the data into subsets based on feature values with the goal of minimizing the impurity within each subset.
2	Random Forest (RF) [16–18]	RF is an ensemble learning method that operates by constructing a multitude of decision trees at training time and outputting the class that is the mode of the classes of the individual trees.
3	XGBoost [19]	XGBoost, which stands for eXtreme Gradient Boosting, is an implementation of the gradient boosting framework that uses a variety of techniques to improve the speed and performance of the model.
4	Multilayer perceptron (MLP) [20]	MLP is a class of feedforward artificial neural network that consists of at least three layers of nodes: an input layer, one or more hidden layers, and an output layer.

The difference between the actual and predicted value is the key to evaluating the adopted model. The evaluation parameters, root mean square error (*RMSE*), mean absolute error (*MAE*), and coefficient of determination (R^2), were selected in this analysis to assess the accuracy of the predicted results, as shown below. The smaller *RMSE*, the higher the accuracy of the predictive model in describing the data. MAE can better reflect the predicted value error. The larger the RR^2, the stronger the interpretability of the predicted value to the actual, and the higher the fitting degree.

$$RMSE = \sqrt{\frac{1}{m}\sum_{i=1}^{m}(y_i - \hat{y}_i)^2} \tag{2.1}$$

$$MAE = \frac{1}{m}\sum_{i=1}^{m}|y_i - \hat{y}_i| \tag{2.2}$$

$$R^2 = 1 - \frac{\sum_{i=1}^{m}(y_i - \hat{y}_i)^2}{\sum_{i=1}^{m}(y_i - \bar{y}_i)^2} \tag{2.3}$$

where i is the data serial number, m is the total number of data, y_i, $\hat{y}_i$, $\bar{y}_i$ are the actual value, predicted value, and mean of actual value, separately.

3. Study area

The database adopted in this work is from the deep foundation pit construction project of a research and development building in Nanjing, with a total area of 10700 m^2. The length of the basement exterior wall is about 430 m, and the excavation depth is 15.1–16.1 m. The south

and north sides of the foundation pit are adjacent to existing municipal roads, pipelines, and buildings. The terrain of the site is relatively flat, with a relative elevation difference of 0.7 m. According to the division of landform units in the Nanjing area, the study area belongs to the terrace landform unit. The excavation area of the foundation pit is mainly filled with land fill, silty clay, silt, and silty sand. The physical and mechanical parameters of the soil from the site, like unit weight (γ), cohesion (c), friction angle (φ), horizontal permeability coefficient (K_h), vertical permeability coefficient (K_v) and compression modulus (E_s), are shown in Table 2.

Table 2. The physical and mechanical parameters of the soil from the study area

Symbol	**Layer**	**γ (kN/m^3)**	**c (kPa)**	**φ (°)**	**K_v (cm/s)**	**K_h (cm/s)**	**E_s (MPa)**
(1)	Land fill	19.0	16.8	11.8	–		5.2
$(2)_1$	Silty clay	19.6	37.8	13.5	–		7.7
$(2)_{1A}$	Silty clay	18.9	20.4	13.8	6.71E-06	8.36E-06	5.2
$(2)_2$	Silt	18.5	6.4	27.9	5.92E-04	6.43E-04	8.1
$(2)_3$	Silt and Silty sand	18.8	6.4	27.8	6.51E-04	6.82E-04	8.9
$(3)_1$	Silty clay and Silt	18.6	11.4	20.8	5.85E-04	6.12E-04	6.1
$(3)_2$	Silty clay	18.8	17.2	17.7	8.41E-06	9.30E-06	4.8
$(3)_3$	Silty clay	19.5	27.8	17.6	7.91E-06	8.52E-06	5.9
(4)	Gravels	20.0	5.0	30	–		–
$(5)_1$	Strongly weathered argillaceous sandstone	21.5	30.0	24	–		–

The types of groundwater on the site are phreatic water, confined water, and bedrock fissure water. The phreatic water is primarily in the layer (1), $(2)_1$, $(2)_{1A}$, and its buried depth was between 2.2–2.6 m below the ground surface. Layer $(2)_1$ and $(2)_{1A}$ serve as the top impermeable layer, while layer $(3)_2$ and $(3)_3$ serve as the bottom impermeable layer. The first layer of confined water aquifer consists of layer $(2)_2$, $(2)_3$, $(3)_1$, which has a high water content, weak permeability, and a large thickness. The second layer of confined water aquifer is in layer (4), which has a moderate water permeability and a thickness of 0.4–3.4 m, with some parts missing.

The design of the excavation wall incorporates drilling and grouting piles, each with a diameter of 1000 mm, arranged with a center-to-center spacing of 1200 mm. These piles are complemented by a reinforced concrete support system, consisting of three discrete layers, to enhance the structural stability and integrity of the wall. The typical cross-section of the foundation pit is shown in Fig. 1. Three-axis deep mixing piles were adopted as a curtain for cutting off water. The total station (Leica TS11+R400) and inclinometer (Hangtian CX-06A) were used to obtain data of the surface settlement and DHD, respectively. The monitoring frequency of all measuring points is once a day during the excavation and construction of deep foundation pits, like surface settlement, deep horizontal displacement (DHD), supporting axial force, etc.

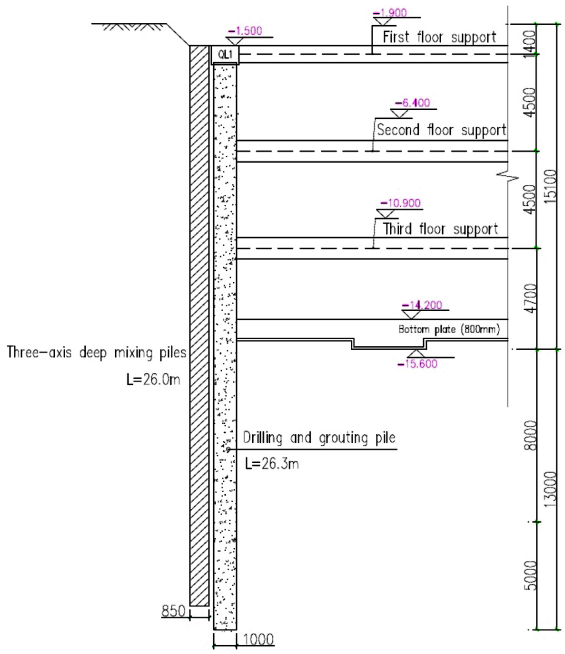

Fig. 1. Typical cross-section of the foundation pit in this work (unit: mm)

4. Sample collection

DHD can describe the horizontal displacement curve of the retaining wall in different directions along the depth, and can timely determine the maximum horizontal displacement and its position. Therefore, the monitoring data of DHD were selected as the prediction object in this study. A total of 13 monitoring points for DHD (CX1–CX13) were set up in this foundation pit. The layout diagram of DHD monitoring points is shown in Fig. 2.

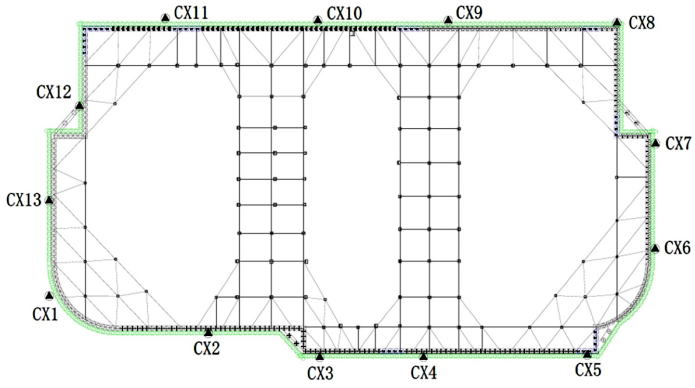

Fig. 2. Layout diagram of DHD monitoring points

Generally, with the continuous excavation and support installation of the foundation pit, the DHD presents different characteristics. In this work, the entire excavation process is divided into three stages, which are crucial for evaluating the stability of deep excavation. The details of three excavation stages are shown in Table 3.

Table 3. The details of three excavation stages

Stage	Depth (m)	Condition
1	5.9	excavate to second floor support
2	10.4	excavate to third floor support
3	15.1	excavate to the bottom of the pit

In this project, the DHD is measured at a vertical distance (0.5 m) interval, and the monitoring data varies at different excavation stages and burial depths. In this way, the depth can be considered as a factor to predict the horizontal displacement. Considering the spatial effect of excavation wall deformation, the spatial position can be divided into two categories based on the plane shape, namely the corner and the straight sections. From Fig. 2, the spatial position of points CX1, CX3, CX5, CX7, CX8, CX12 belongs to the corners, while points CX2, CX4, CX6, CX9, CX10, CX11 are classified as straight sections. In addition, Due to the similar hydrogeological conditions of each measuring point based on the survey results, it is assumed that the hydrogeological conditions of each measuring point have a consistent impact on DHD. Therefore, the hydrogeological conditions have not been considered as influencing factor in this study.

Based on the above analysis, only three factors, namely excavation depth (ED), spatial position (SP), and buried depth (BD) are selected as the features to build sample data. 1362 sets of data were obtained from the above 12 monitoring points for DHD. The statistical description of the dataset is shown in Table 4.

Table 4. Statistical description of the dataset

Feature	Avg.	Std.	Min.	Max.
Input				
ED (m)	10.39	3.74	5.90	15.10
SP	1.54	0.50	1.00	2.00
BD (m)	12.57	7.13	0.50	25.00
Output				
DHD (mm)	5.64	5.96	–0.40	19.60

5. Results and discussion

Due to the difficulty in determining parameters, the grid search optimization method was adopted to determinate various parameters for all five models. 70% of the sample data is used to train the model, and the rest for testing. Based on five-fold cross validation, the evaluation results can be obtained as shown in Table 5.

Table 5. Evaluation results of four machine-learning algorithms

Algorithm	***RMSE***	***MAE***	R^2
MLP	2.4167	1.6029	0.8941
DT	2.4635	1.6619	0.8984
RF	2.3700	1.5940	0.9063
XGBoost	2.3397	1.5732	0.9088

From Table 5, the XGBoost algorithm has the highest R^2 and lowest *RMSE* and *MAE* among the four algorithms. The actual-predicted test values from XGBoost algorithm are shown in Fig. 3, from which most of the points are concentrated in the vicinity of the red straight line, also reflect its good predictive performance. What's more, it can be seen that only three simple factors are considered in the models, the R^2 of all mainstream machine-learning algorithms can achieve about 0.9. In this way, the machine-learning algorithms can be a great tool for predicting DHD caused by deep excavation. Figure 4 plots the heat map of correlation coefficients of selected three factors. The correlation between factors is very small, between –0.04 and 0.3, indicating the rationality of feature selection.

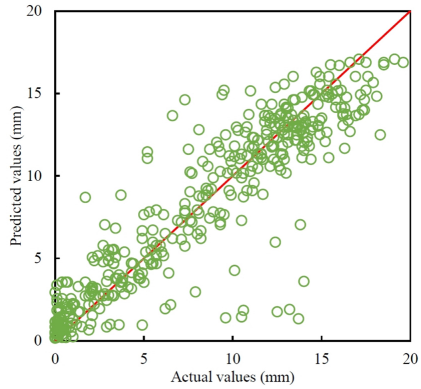

Fig. 3. Actual-predicted test values from XGBoost algorithm

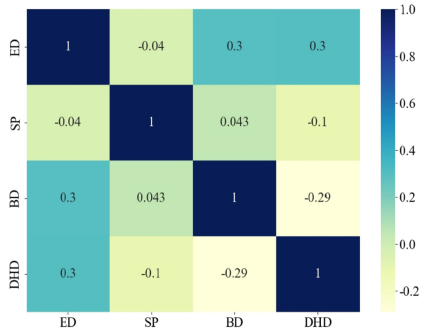

Fig. 4. Heat map of correlation coefficients of selected factors

Based on the predicted results from XGBoost algorithm, the accuracy of different excavation stages is presented in Fig. 5, from which the stage 2 has the highest R^2, and lowest *RMSE* and *MAE*. The accuracy of stage 1 is relatively poor, the R^2 is 0.8318 in this stage. Therefore, the XGBoost algorithm can describe the DHD of excavation wall in different excavation stages with three simple factors.

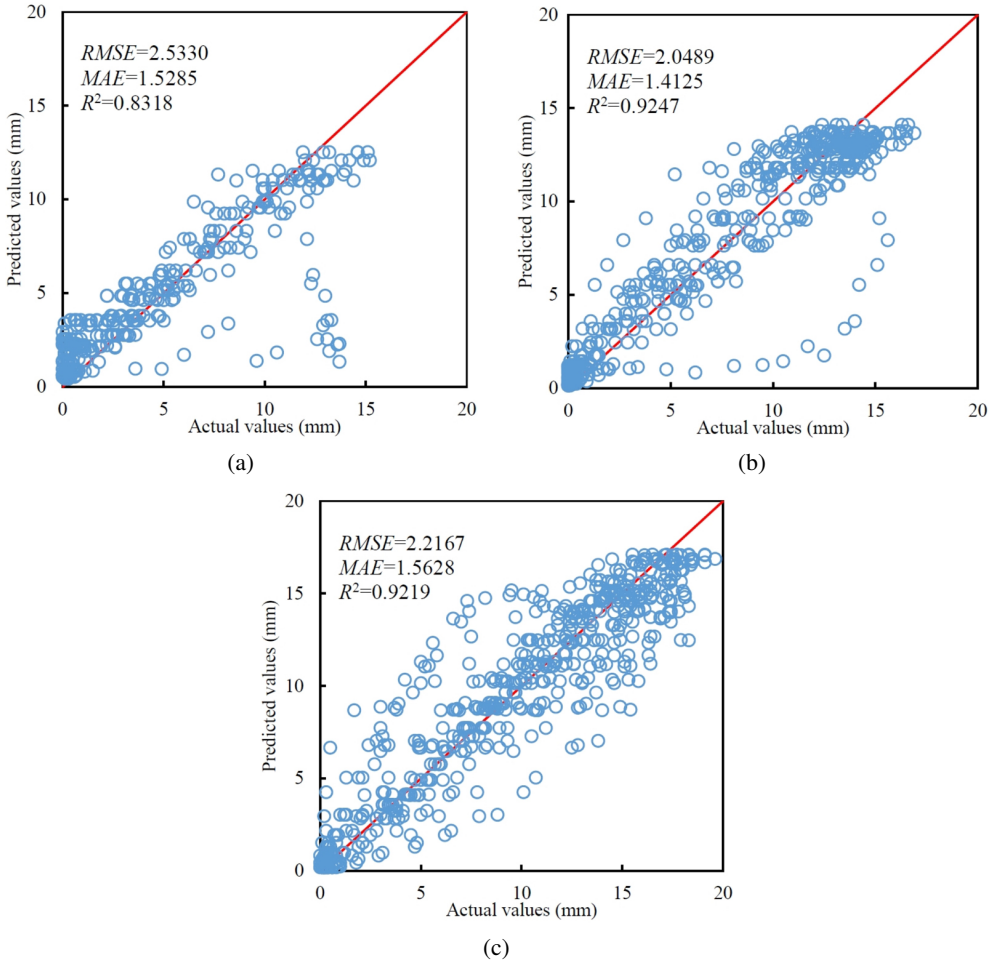

Fig. 5. Actual-predicted values from different excavation stages: (a) Stage 1; (b) Stage 2; (c) Stage 3

Figure 6 plots the actual-predicted values from different spatial position. From Fig. 6(a), the R^2 in corners reach 0.9597, *RMSE* and *MAE* are 1.6399 and 1.217, respectively, which are better than the accuracy at straight sections. It can be seen that the XGBoost algorithm can predict the DHD at corners more accurate than the straight sections.

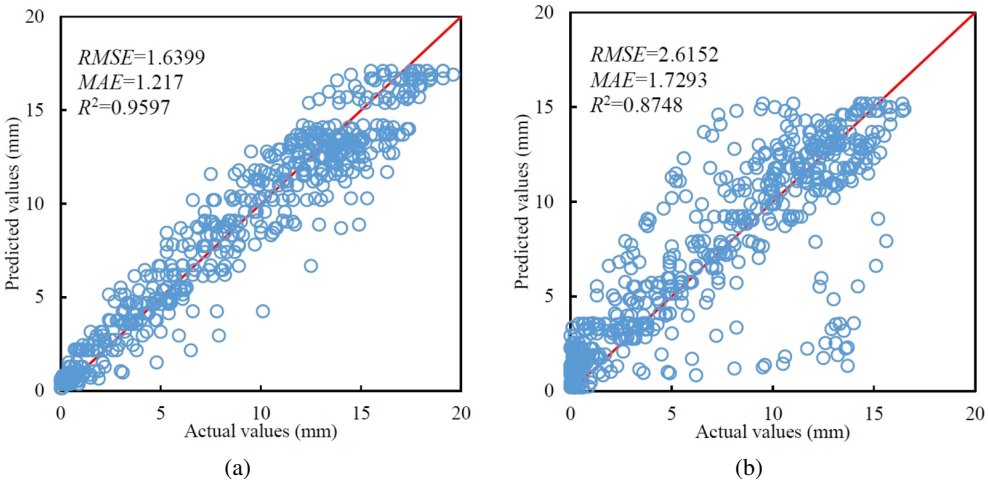

Fig. 6. Actual-predicted values from different spatial position: (a) Corners; (b) Straight sections

Figure 7 presents the actual and predicted DHD of the excavation wall at the monitoring point CX8 in different stages. From Fig. 7, both the DHD numerical values and the overall trend show good consistency between the predicted values calculated by the XGBoost algorithm and the actual monitoring values. The *RMSE*, *MAE*, and R^2 are 1.5710, 1.3207, and 0.9683, respectively, which also verify the feasibility of machine-learning algorithms for predicting DHD caused by deep excavation.

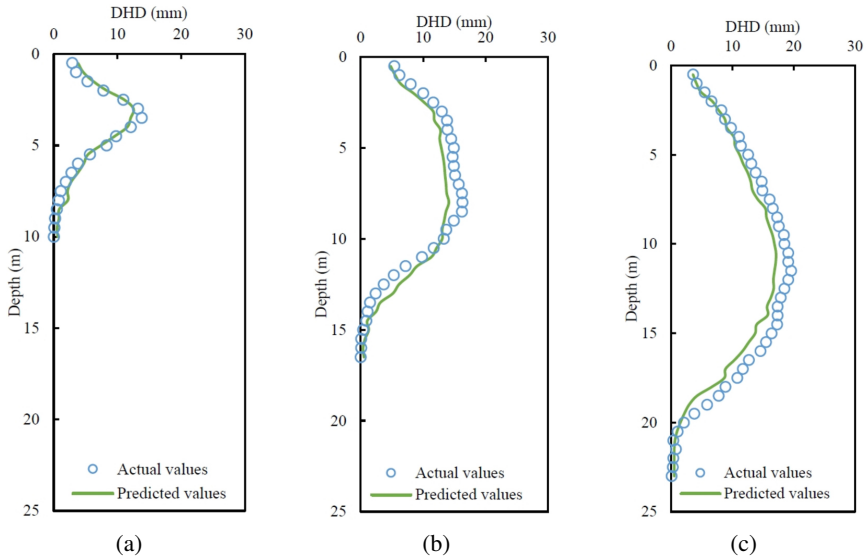

Fig. 7. Actual-predicted values of DHD at CX8 in different stages: (a) Stage 1; (b) Stage 2; (c) Stage 3

6. Conclusions

In order to predict the DHD of excavation wall induced by deep excavation, four machine-learning algorithms (MLP, DT, RF, and XGBoost) were employed to build prediction models, which include three simple influencing factors, namely ED, SP, and BD. *RMSE*, *MAE*, and R^2 were introduced to evaluate the accuracy of the model. Verified by a dataset of 1362, the XGBoost algorithm has the best performance for predicting DHD with an *RMSE* of 2.3397, an *MAE* of 1.5732 and R^2 of 0.9088. In addition, the accuracy is relatively higher predicted by XGBoost algorithm at the corners than these at straight sections. From the perspective of excavation process, the prediction accuracy of the excavation stage 2 is better than that of the stage 1 and 3.

In sum, the application process for predicting DHD based on machine-learning algorithms in this work has great potential for promotion in practical engineering project, more data and factors may be needed to further improve prediction accuracy. In addition, only the geometric parameters are considered as input data in the work, the geotechnical conditions also have obvious influence on the foundation pit stability. Hence, it is significant to take geotechnical parameters into account in further research.

References

[1] Y.S. Deng, et al., "Failure analysis and zoning control of water gushing in foundation pit", *Engineering Failure Analysis*, vol. 145, art. no. 107029, 2023, doi: 10.1016/j.engfailanal.2022.107029.

[2] K.K. Phoon and W. Zhang, "Future of machine learning in geotechnics", *Georisk: Assessment and Management of Risk for Engineered Systems and Geohazards*, vol. 17, no. 1, pp. 7–22, 2023, doi: 10.1080/17499518.2022.2087884.

[3] M. Azadi, S. Pourakbar, and A. Kashfi, "Assessment of optimum settlement of structure adjacent urban tunnel by using neural network methods", *Tunnelling and Underground Space Technology*, vol. 37, pp. 1–9, doi: 10.1016/j.tust.2013.03.002.

[4] K. Ahangari, S.R. Moeinossadat, and D. Behnia, "Estimation of tunnelling- induced settlement by modern intelligent methods", *Soils and Foundations*, vol. 55, no. 4, pp. 737–748, 2015, doi: 10.1016/j.sandf.2015.06.006.

[5] S. Acikgoz, K. Soga, and J. Woodhams, "Evaluation of the response of a vaulted masonry structure to differential settlements using point cloud data and limit analyses", *Construction and Building Materials*, vol. 150, pp. 916–931, 2017, doi: 10.1016/j.conbuildmat.2017.05.075.

[6] M. Rajabi, R. Rahmannejad, M. Rezaei, and K. Ganjalipour, "Evaluation of the maximum horizontal displacement around the power station caverns using artificial neural network", *Tunnelling and Underground Space Technology*, vol. 64, pp. 51–60, 2017, doi: 10.1016/j.tust.2017.01.010.

[7] J. Zhou, X.Z. Shi, K. Du, X.Y. Qiu, X.B. Li, and H.S. Mitri, "Feasibility of random-forest approach for prediction of ground settlements induced by the construction of a shield-driven tunnel", *International Journal of Geomechanics*, vol. 17, no. 6, art. no. 04016129, 2017, doi: 10.1061/(ASCE)GM.1943-5622.0000817.

[8] W. Zhang, Y. Li, A.T.C. Goh, and R. Zhang, "Numerical study of the performance of jet grout piles for braced excavations in soft clay", *Computers and Geotechnics*, vol. 124, art. no. 103631, 2020, doi: 10.1016/j.compgeo.2020.103631.

[9] R. Zhang, C. Wu, A.T.C. Goh, T. Bohlke, and W. Zhang, "Estimation of diaphragm wall deflections for deep braced excavation in anisotropic clays using ensemble learning", *Geoscience Frontiers*, vol. 12, no. 1, pp. 365–373, 2021, doi: 10.1016/j.gsf.2020.03.003.

[10] C. Jing, H. Wang, and H. Li, "Deformation prediction of foundation pit based on exponential power product model of improved algorithm", *Geofluids*, art. no. 7055693, 2021, doi: 10.1155/2021/7055693.

[11] H. Li, Z. Zhao, and X. Du, "Research and application of deformation prediction model for deep foundation pit based on LSTM", *Wireless Communications and Mobile Computing*, art. no. 9407999, 2022, doi: 10.1155/2022/9407999.

[12] A.Z.O. Al-Hijazeen, M. Fawad, M. Gerges, K. Koris, and M. Salamak, "Implementation of digital twin and support vector machine in structural health monitoring of bridges", *Archives of Civil Engineering*, vol. 69, no. 3, pp. 31–47, 2023, doi: 10.24425/ace.2023.146065.

[13] Y. Xu, Y. Zhao, Q. Jiang, J. Sun, C. Tian, and W. Jiang, "Machine-Learning-Based deformation prediction method for deep foundation-pit enclosure structure", *Applied Sciences*, vol. 14, no. 3, art. no. 1273, 2024, doi: 10.3390/app14031273.

[14] J.R. Quinlan, "Induction of decision trees", *Machine Learning*, vol. 1, no. 1, pp. 81–106, 1986, doi: 10.1007/BF00116251.

[15] H.R. Luo, F. Cheng, H. Yu, and Y.Q. Yi, "SDTR: soft decision tree regressor for tabular data", *IEEE Access*, vol. 9, pp. 55999–56011, 2021, doi: 10.1109/ACCESS.2021.3070575.

[16] L. Breiman, "Random Forests", *Machine Learning*, vol. 45, no. 1, pp. 5–32, 2001, doi: 10.1023/A:1010933404324.

[17] M. Schonlau and R.Y. Zou, "The random forest algorithm for statistical learning", *The Stata Journal: Promoting Communications on Statistics and Stata*, vol. 20, no. 1, pp. 51–94, 2020, doi: 10.1177/1536867X209096.

[18] J. Dzięcioland W. Sas, "Estimation of the coefficient of permeability as an example of the application of the Random Forest algorithm in Civil Engineering", *Archives of Civil Engineering*, vol. 70, no. 2, pp. 119–134, 2024, doi: 10.24425/ace.2024.149854.

[19] T. Chen and C. Guestrin, "XGBoost: A scalable tree boosting system", in *KDD '16: Proceedings of the 22nd ACM SIGKDD International Conference on Knowledge Discovery and Data Mining*. New York: ACM, 2016, pp. 785–794, doi: 10.1145/2939672.2939785.

[20] M.I. Dutt and W. Saadeh, "Multilayer perceptron (MLP) regressor network for monitoring the depth of Anesthesia", in*Proceedings of the 2022 20th IEEE Interregional NEWCAS Conference NEWCAS*). IEEE, 2022, pp. 251–255, doi: 10.1109/NEWCAS52662.2022.9842242.

Received: 2024-07-22, Revised: 2024-09-21